

# Damage Mechanics of Porcine Flexor Tendon: Mechanical Evaluation and Modeling

SARAH DUENWALD-KUEHL,<sup>1</sup> JACLYN KONDRATKO,<sup>1,2</sup> RODERIC S. LAKES,<sup>2,3</sup> and RAY VANDERBY JR.<sup>1,2</sup>

<sup>1</sup>Department of Orthopedics and Rehabilitation, University of Wisconsin-Madison, 1111 Highland Ave, WIMR 5059, Madison, WI 53705, USA; <sup>2</sup>Department of Biomedical Engineering, University of Wisconsin-Madison, Madison, WI, USA; and <sup>3</sup>Department of Engineering Physics, University of Wisconsin-Madison, Madison, WI, USA

(Received 16 November 2011; accepted 23 February 2012; published online 8 March 2012)

Associate Editor Michael R. Torry oversaw the review of this article.

**Abstract**—Porcine flexor tendons underwent cyclic and stress relaxation testing before and after strain exceeding elastic limit (“overstretch”) to examine which mechanical parameters undergo changes following subfailure damage. From these data, we developed an “effective strain” damage model (in which the tendon is modeled as if being pulled to a lower strain). Damage was induced at three strain levels to determine the extent to which post-damage parameter changes were affected by overstretch strain level. We found that diffuse damage induced by overstretch decreased elastic and viscoelastic parameters obtained during testing. The stress response of tendon to strain is therefore altered following damage. We next compared the strain-dependent parameter behavior to damage-dependent behavior to determine the effective strain for each parameter. Effects of damage became more pronounced as strain during overstretch increased; following overstretch to 6.5, 9, or 13% strain, effective strain was  $2.43 \pm 0.33$ ,  $1.98 \pm 0.3$ , or  $0.88 \pm 0.43\%$  strain, respectively. By determining the effective strain and using it to calculate predicted values of post-damage mechanical parameters, it was possible to predict the stress relaxation behavior of tendons with Schapery’s non-linear viscoelastic model. Using this approach, a single parameter predicts both elastic and viscoelastic compromise from known, strain-dependent behaviors.

**Keywords**—Tendon, Damage, Mechanics, Equivalent strain.

## INTRODUCTION

Tendons are essential to move joints, absorb impacts, and store energy during loading to facilitate efficient movement. The ability of tendons to perform these functions is connoted by their mechanical

properties. Though typically able to withstand normal movement and activities, tendons can be injured during abnormal movement or chronic loading. Tendons that have undergone subfailure damage have compromised mechanical properties<sup>8,9</sup> and therefore have compromised ability to carry out normal functions (i.e., joint movement and stabilization). Biological and mechanical metrics can quantify damage<sup>9</sup>; altered mechanical properties provide a direct measure of functional compromise. Therefore, by anticipating changes in mechanical properties resulting from such damage, it is possible to anticipate alterations in tendon function.

Tendons with subfailure damage have different biomechanical behavior than normal tissues, including both elastic and viscoelastic (or time-dependent) changes. Damage can lead to a drop in load for a given strain<sup>4,13</sup> or differences in viscoelastic properties.<sup>9</sup> “Damage” in this study is defined as changes in the microstructure of tendon that lead to a reduction in its mechanical strength,<sup>4,13</sup> and is caused by “overstretch,” which is defined as the application of strain states that exceed the tendon’s elastic limit.<sup>8</sup> The elastic limit was determined to be 6% strain, as this is the highest strain at which we were able to perform repeatable testing<sup>1</sup> and is consistent with reported upper bounds on the physiologic range.<sup>3,7</sup> The healing response to damage can compromise function in many ways. Adhesions limit range of joint motion. Scar formation can alter load distribution and mechanical properties to potentially result in tearing of tendon, insertion sites, or even adjacent muscle tissue. Conversely, increased laxity from overstretch could allow hypermobility of the joint or require altered neuromuscular control to facilitate precise movements. Changes in viscoelastic properties could result in

Address correspondence to Ray Vanderby Jr., Department of Orthopedics and Rehabilitation, University of Wisconsin-Madison, 1111 Highland Ave, WIMR 5059, Madison, WI 53705, USA. Electronic mail: vanderby@ortho.wisc.edu, duenwald@wisc.edu

differences in how tendons cope with impact or prolonged loading scenarios, or how they return potential energy to facilitate movement. Even subtle differences in tendon mechanical behavior may predict accumulation of damage and pathologic sequelae.

The stress response of a tendon to strain is the fundamental mechanical behavior of the tissue. A strain-based continuum mechanics characterization of damage suggests that the stress associated with the damaged state under an applied strain is equivalent to the stress associated with its undamaged state under effective strain.<sup>13</sup> In other words, the strain-dependent mechanical behavior (constitutive functions) of the tendon are unaltered if one calculates the response based on the effective strain rather than the applied strain (see Fig. 1). Therefore, if the relationship between the effective strain and the applied strain is known, as well as the strain-dependence of the mechanical parameters of interest, it is possible to anticipate the changes in mechanical properties resulting from damage and predict functional compromise.

In this study we set out to examine the effects of damage on the mechanical behavior of tendon by subjecting tendons to cyclic and stress relaxation testing prior to and following overstretch damage. The damage mode, subfailure damage caused by overstretching the tendon beyond its elastic limit, is representative of the strain and sprain injuries that affect tendons and ligaments during abnormal movement and flexion events. Studying and modeling the effects of such damage allows for a better understanding of the compromised function of the tissues associated with the residual laxity following overstretch injuries and may give insight to the high incidence of re-injury

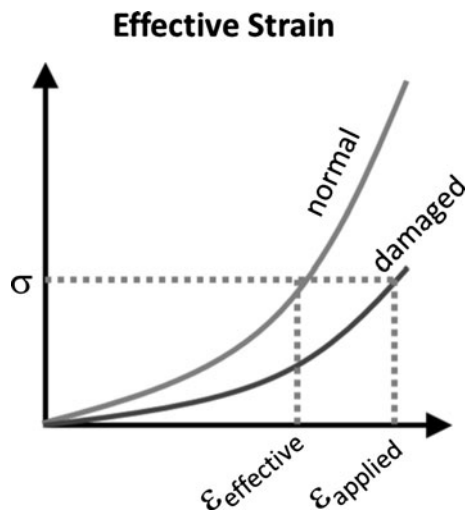


**FIGURE 1.** Strain-based approach to damage description. The stress at the applied strain ( $\epsilon_{\text{applied}}$ ) on the damaged stress-strain curve is equivalent to the stress at the effective strain ( $\epsilon_{\text{effective}}$ ) on the normal stress-strain curve.

and long recovery times. The overall goals are: (1) determine which viscoelastic and elastic mechanical parameters can quantify subfailure damage in overstretched tendon and (2) use these parameters to model post-damage behavior; specific objectives included in this second goal include: (a) partnering strain-dependent parameter analysis with the mechanical results in order to (b) determine the “effective strain” of each parameter after each damage case, and (c) use these results to build a predictive model of damage behavior based on the effective strain principle. We hypothesize that increasing strain during damage-causing overstretch will lower the effective strain; in other words, increased damage in the tissue will lead to increased tendon laxity, which results in parameter values similar to those at lower strains in pre-damage tests.

## MATERIALS AND METHODS

### *Specimen Preparation*

Thirty-five porcine digital flexor tendons (3rd and 4th digit) were excised from 18 forelimbs obtained from a local abattoir with care to leave the bony insertion sites intact at the distal ends of the tendons. Specimens were kept hydrated in physiologic buffered saline until loading into the mechanical test system. Bony ends were then potted in lightweight polyester resin filler molded to fit inside a stainless steel bone block. Unloaded cross-sectional area was measured assuming an elliptical shape; long and short axes were measured at three points along the tendon and averaged.

Specimens were loaded into custom grips in a PBS-filled bath in the servohydraulic test system (Bionix 858, MTS, Minneapolis, MN). The muscle end of the tendons was secured in a custom soft tissue grip, with a pan for holding dry ice (freezing of the soft tissue end helps prevent slippage) and a connection to the moving crosshead of the servohydraulic machine. The potted bony ends were enclosed in a stainless steel grip fixed to the test frame. Grip-to-grip displacement was controlled by the servohydraulic machine and load was measured using a 1000 lb load cell (Honeywell, Morristown, NJ). Data were captured on a PC equipped with Labtech Notebook (Laboratory Technology Corporation, Fort Collins, CO).

Once in the test frame, specimens were preloaded to 1 N (to remove slack in the tendon) and initial tendon length,  $L_0$ , was measured for strain calculations using digital calipers. Tendons were preconditioned using a sinusoidal wave from 0 to 2% strain at 0.5 Hz for 20 s. Tendons were allowed to rest for 1000 s prior to further mechanical testing to allow for complete recovery.

### Mechanical Testing: Objective 1

Specimens were randomly assigned to subfailure ( $n = 30$ ) or strain-dependent ( $n = 5$ ) testing. In the subfailure testing, stress relaxation and cyclic testing were performed prior to and following overstretch damage to quantify the mechanical changes following damage. Stress relaxation (40 ms ramp, held 100 s, 40 ms return to zero) and cyclic testing (0.5 Hz for 20 s between 0 and 4%) were performed on tendons with 1000 s rest periods at zero strain between each test. Data were sampled at a rate of 10 Hz. Two relaxation tests and two cyclic tests were performed on each specimen prior to inducing damage, which was done using an overstretch pull (in % strain) to 6.5 ( $n = 10$ ), 9 ( $n = 10$ ), or 13 ( $n = 10$ ) in 1 s. These strains were chosen to fall outside of the normal maximum physiologic strain of 5–6%<sup>3,7</sup> but below reported failure strains of 15–20%.<sup>5,12</sup> Following this overstretch (and a 1000 s rest period at zero strain), relaxation tests and cyclic tests were repeated.

### Mechanical Testing: Objective 2a

In strain-dependent testing, five tendons were selected to undergo stress relaxation testing at various strains in order to ascertain the strain dependence of mechanical parameters associated with stress relaxation. Tendons were subjected to stress relaxation at 1, 2, 3, 4, 5, and 6% strain for 100 s (in random order) with 1000 s rest at zero strain between each relaxation test to allow for viscoelastic recovery.

### Parameter Calculation: Objective 1

To fulfill our primary goal (determining which viscoelastic and elastic mechanical parameters can quantify subfailure damage in overstretched tendon) mechanical parameters were calculated from the gathered data. Force data ( $F$ ) acquired by the servohydraulic system during stress relaxation testing were divided by original cross-sectional area,  $a_0$ , to calculate stress ( $\sigma$ ).

$$\sigma(t) = F(t)/a_0 \quad (1)$$

Stress data were then used to calculate parameters of interest (Fig. 2a) such as the maximum stress reached during stress relaxation ( $\sigma_{\text{max-rlx}}$ ) and the reduction in stress during relaxation ( $\sigma_{\text{decay-rlx}}$ ), both prior to and following damage. Stress data were also used to calculate  $E(t)$  (relaxation modulus) results by dividing stress by input strain;

$$E(t) = \sigma(t)/\varepsilon_0 \quad (2)$$

the resulting  $E(t)$  results were fit with a power law and parameters  $A$  and  $n$  were calculated before and after damage.

$$E(t) = At^n \quad (3)$$

Time-dependent behaviors were fit with Schapery's viscoelastic model,<sup>2,11</sup> and model parameters  $h_e$  and  $h_2$  were calculated. Schapery's nonlinear viscoelastic model is defined as:

$$\sigma(t) = h_e E_e + h_1 \int_0^t \Delta E(\rho - \rho') \frac{dh_2}{d\tau} d\tau \quad (4)$$

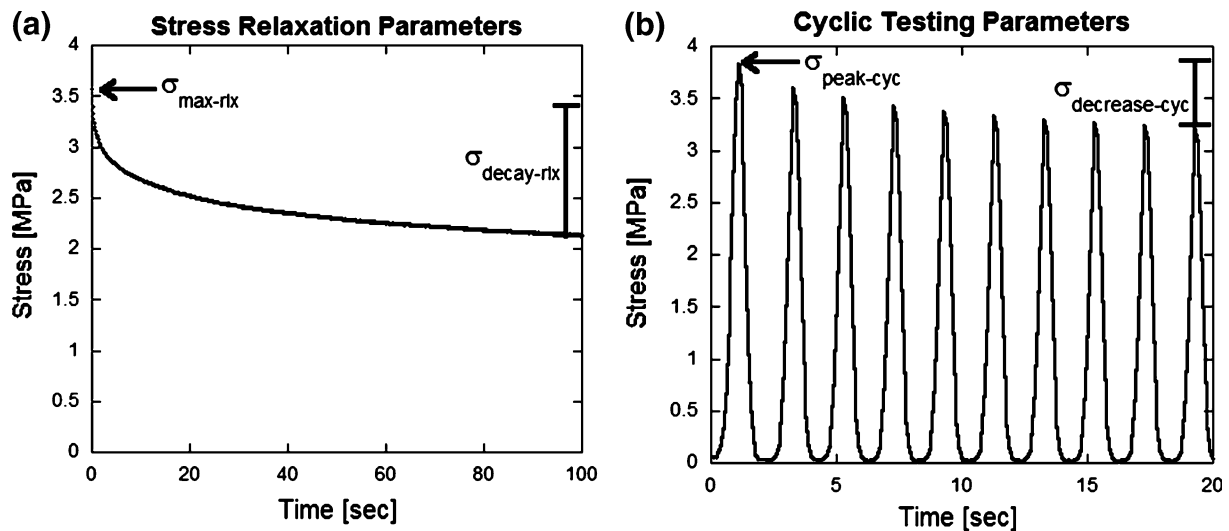


FIGURE 2. Mechanical parameters of interest from (a) stress relaxation testing:  $\sigma_{\text{max-rlx}}$  (maximum stress reached) and  $\sigma_{\text{decay-rlx}}$  (decrease in stress over 100 s) and (b) cyclic testing:  $\sigma_{\text{peak-cyc}}$  (peak stress reached) and  $\sigma_{\text{decrease-cyc}}$  (decrease in peak stress over 10 cycles).

where  $h_e$ ,  $h_1$ , and  $h_2$  are strain-dependent material properties related to Helmholtz free energy (specifically, 3rd order and higher strain effects),  $\Delta E$  is the transient component of the modulus (defined by  $\Delta E \equiv E(t) - E_e$ ),  $E_e$  is the equilibrium or final value of the modulus (defined by  $E_e = E(\infty)$ ), and  $\rho$  and  $\rho'$  are defined as follows:

$$\rho \equiv \int_0^t dt' / a_e[\varepsilon(t')] \quad (a_e > 0). \quad (5)$$

$$\rho' \equiv \rho(\tau) = \int_0^\tau dt' / a_e[\varepsilon(t')]. \quad (6)$$

where  $a_e$  is an additional strain-dependent material property related to strain influences in free energy and entropy production.<sup>11</sup> Physically,  $\rho$  can be regarded as an internal clock time which can depend on strain. Testing tendon and ligament in isothermal conditions results in  $h_1$  and  $a_e$  becoming 1,<sup>11</sup> so the equation becomes:

$$\sigma(t) = [h_e E_e + h_2 \Delta E(t - t_a)]\varepsilon \quad (7)$$

and the key parameters for model construction are  $h_e$  and  $h_2$ .

Force data acquired during cyclic testing were also used to calculate stress data, and displacement data were used to calculate strain as a function of time (by dividing grip-to-grip displacement by initial length,  $L_0$ ), such that stress–strain curves could be generated prior to and following damage. Stress data were then used to calculate parameters of interest (Fig. 2b) such as the peak stress reached during cyclic testing ( $\sigma_{\text{peak-cyc}}$ ) and the decrease in peak stress from the first to last cycle ( $\sigma_{\text{decrease-cyc}}$ ), prior to and following damage. In addition, the strain at initial loading ( $\varepsilon_{0+}$ ) was calculated by recording the strain required to increase the load (from the 1 N preload) by 0.06 N (the smallest load increment that can be distinguished from noise, based on the sensitivity of the load cell). The stress–strain curve from the first half-cycle (0–4% strain) was then fit with a 3rd-order polynomial (the lowest-order polynomial with  $R^2$  values consistently greater than 0.9) such that the first and second derivatives (representing slope and curvature, respectively) could be calculated at a point along the curve (2% strain was chosen as a point which had a reliably non-zero slope, even after the damage pull, and is a physically relevant strain). Post-damage to pre-damage ratios were then calculated for each parameter (values from the two trials for each specimen were averaged) in order to compare damage affects at each overstretch strain level.

### Parameter Interrelationships: Objective 1

To examine the interrelationships, each pair of parameters was plotted and fitted with a linear curve fit and the  $R^2$  value calculated. Correlation strength was defined by  $R^2$  values: strong correlations had  $R^2$  values greater than 0.8, correlations greater than 0.6, and weak correlations greater than 0.4.

### Effective Strain Calculation: Objective 2b

Parameter values calculated for each strain level from mechanical data (see “Mechanical Testing: Objective 2a” section) were normalized by the value at 4% strain (the strain at which pre- and post-damage cyclic and relaxation testing occurred) and averaged. Plots of normalized parameter versus strain were then generated, and the resulting curves were fit with a third-order polynomial (of the form  $y = ax^3 + bx^2 + cx + d$ ), which was chosen for its ability to fit varying parameter trends with high  $R^2$  values. The resulting equations gave a relationship between strain ( $x$ ) and normalized parameter ratio value ( $y$ ). Mechanical data from experiments (post-damage value normalized by pre-damage value at 4% strain) were then used as  $y$  values in the third-order polynomial equations to solve for  $x$ , which is the “effective strain” value (see following section, Fig. 1). Effective strains for each overstretch strain level (6.5, 9, and 13% strain) were averaged across parameters.

### Model Calculations: Objective 2c

Damage models in this study were built upon the idea that the stress in the tissue (and resulting parameters) are a function of *effective* strain rather than *applied* strain. Effective strain can be related to applied strain through the following equation:

$$\varepsilon_{\text{eff}} = [1 - D]\varepsilon_{\text{app}} \quad (8)$$

where  $\varepsilon_{\text{eff}}$  refers to the effective strain,  $\varepsilon_{\text{app}}$  refers to the applied strain, and  $D$  is the damage parameter that relates to the damage state of the tissue. In the case of strains below the elastic limit of the tissue,  $D$  is equal to 0, and the effective strain is equal to the applied strain. In the case of strains above the elastic limit of the tissue,  $D$  increases with increased damage in the tissue, and thus the effective strain is smaller than the applied strain.

The formation of damage parameters has been achieved in many ways. Some relate damage to the reduction of structural support, based on the amount of remaining intact material. For example, Natali *et al.*<sup>8</sup> defined damage in tendon,  $D_f$ , as a ratio of the number of fibers that had failed at a given stretch to the total number of fibers in the tissue:

$$D_f = \frac{\# \text{ fibers failed at stretch}}{\text{total } \# \text{ fibers in tissue}} \quad (9)$$

Additionally, Lemaitre defined a damage variable associated with the normal direction,  $D_n$ , as the difference between the overall area of the material and the effective resisting area divided by the overall area of the material<sup>6</sup>:

$$D_n = \frac{S - \bar{S}}{S} \quad (10)$$

where  $S$  is the overall area of the material section and  $\bar{S}$  is the effective resisting area.

Others relate damage to altered mechanical performance, based on post-damage mechanical response to load. For example, a structural damage parameter,  $D_s$ , was defined by Provenzano *et al.*,<sup>10</sup> which related the initial length of tendon (at preload) to the length of tendon (at preload) following damage:

$$D_s = 100 \left[ \frac{L_s - L_0}{L_0} \right] \quad (11)$$

where  $L_s$  is the length of the tendon following damage and  $L_0$  is the initial length of the tendon.

The damage parameter in Eq. (9) is well suited for computer models of tendon behavior, with histologic input. However, it is difficult to know the exact number of fibers in a specimen as well as the number of fibers that have failed during practical mechanical testing, and it would require the use of certain imaging modalities (i.e., TEM and SEM) to help form estimates of fiber numbers. Likewise, the parameter in Eq. (10) could be readily computed using a computer model or, alternatively, if damage was induced by cutting through a portion of the cross-sectional area (thus leaving a well-defined intact effective resisting area). Diffuse damage, however, leaves a less easily calculated effective resisting area (again, requiring imaging modalities to help form estimates of intact area). Conversely, the damage parameter in Eq. (11) is easy to relate directly to mechanical testing outcomes, particularly if testing is done in a load-controlled manner. A similar construction of the damage parameter was used in this study.

When a controlled experiment is performed, the input strain is known, and therefore one metric with which damage can be predicted is the input strain itself, provided the elastic limit is known or can be determined. Therefore, an empirical damage parameter is:

$$\begin{aligned} \text{for } \varepsilon \leq \text{elastic limit} \quad D_{\text{empirical}} &= 0 \\ \text{for } \varepsilon > \text{elastic limit:} \quad D_{\text{empirical}} &= C(\text{input strain}) \end{aligned} \quad (12)$$

where  $C$  is a constant that needs to be calculated empirically (in this case, by plotting the ratio of effective strain to applied strain).

If the input strain is not known, the stress–strain curve following damage can be compared to the pre-damage curve (or a reference curve for the tissue) provided the curves were constructed under the same conditions (i.e., same strain rate) to predict the mechanical properties following damage. If the slopes of the stress–strain curves are compared (in this case, the slope is taken at 2%), the resulting damage parameter can be calculated:

$$\begin{aligned} \text{for } \varepsilon \leq \text{elastic limit} \quad D_{\text{slope}} &= 0 \\ \text{for } \varepsilon > \text{elastic limit:} \quad D_{\text{slope}} &= 1 - \frac{d'|_{2\%, \text{post-damage}}}{d'|_{2\%, \text{pre-damage}}} \end{aligned} \quad (13)$$

where  $d'|_{2\%}$  represents the slope of the stress–strain curve at 2% strain.

So, for the model calculations in this study, we have:

$$\varepsilon_{\text{eff}} = 0.04[1 - C(\text{input strain})] \quad (14)$$

and

$$\varepsilon_{\text{eff}} = 0.04 \left[ \frac{d'|_{2\%, \text{post-damage}}}{d'|_{2\%, \text{pre-damage}}} \right] \quad (15)$$

to describe post-damage effective strain levels. The strain-dependence information about the parameters can then be used to calculate post-damage parameters for use in Schapery's nonlinear viscoelastic constitutive model (Eqs. 4–7). For more information about the use of Schapery's nonlinear viscoelastic model, see Duenwald *et al.*<sup>2</sup> and Schapery.<sup>11</sup>

### Statistical Analysis

Post-damage to pre-damage ratios of parameters following overstretch to 6.5, 9, and 13% strain were compared using a repeated measures ANOVA. Percent errors for each Schapery model prediction (data-based, empirical-model-based, and slope-model-based) were compared using a repeated measures ANOVA. Statistical significance was chosen to be  $p \leq 0.05$ .

## RESULTS

### Mechanical Evaluation: Objective 1

Subjecting tendons to overstretch strains led to diffuse damage in the tissue manifested in the mechanical testing as reduced stress at a given strain in the stress–strain curve (Fig. 3a), a rightward shift in the stress–strain curve and increased strain at initial loading (Fig. 3b), reduced stress levels and reduced

stress decrease during cyclic testing (Fig. 3c), and reduced stress levels and reduced stress decay during stress relaxation testing (Fig. 3d).

The cyclic testing parameters  $\sigma_{\text{decrease-cyc}}$  and  $\sigma_{\text{peak-cyc}}$  both decreased following damage (Fig. 4a). Post-damage to pre-damage ratios of  $\sigma_{\text{decrease-cyc}}$  (mean  $\pm$  standard deviation) were  $0.23 \pm 0.07$ ,  $0.15 \pm 0.05$ , and  $0.04 \pm 0.02$  following overstretch at 6.5, 9, and 13% strain, respectively; each overstretch strain level was significantly different than the others ( $p = 0.0094$ ). Post-damage to pre-damage ratios of  $\sigma_{\text{peak-cyc}}$  following 6.5, 9, and 13% strain were  $0.56 \pm 0.09$ ,  $0.34 \pm 0.10$ , and  $0.12 \pm 0.05$ , respectively, and each

overstretch level was significantly different than the others ( $p = 0.0039$ ).

Stress relaxation parameters  $\sigma_{\text{max-rlx}}$  and  $\sigma_{\text{decay-rlx}}$  decreased following overstretch (Fig. 4b). Post-damage to pre-damage ratios of  $\sigma_{\text{max-rlx}}$  following pull to 6.5, 9, and 13% strain were  $0.66 \pm 0.08$ ,  $0.43 \pm 0.10$ , and  $0.14 \pm 0.07$ , respectively, and each overstretch level was significantly different than the others ( $p = 0.0031$ ). Similarly, the post-damage to pre-damage ratios of  $\sigma_{\text{decay-rlx}}$  following pull to 6.5, 9, and 13% strain were  $0.64 \pm 0.10$ ,  $0.41 \pm 0.10$ , and  $0.14 \pm 0.09$ , respectively. Each overstretch strain level was significantly different than the others ( $p = 0.0037$ ).

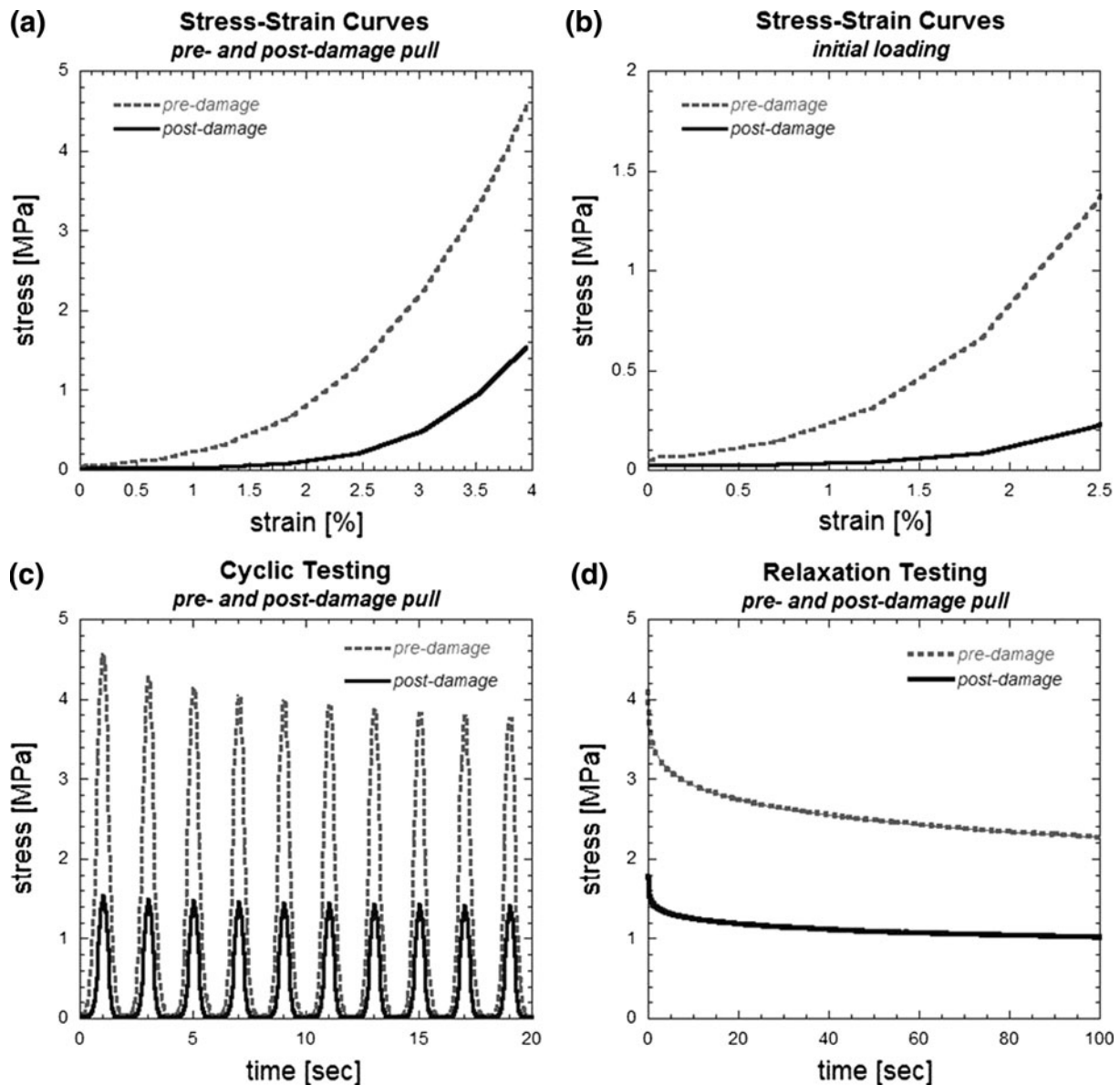


FIGURE 3. Representative pre-damage and post-damage results for a specimen subjected to an overstretch at 9% strain; damage is manifested in (a) lower stresses and less curvature in the stress–strain curve, (b) rightward shift in initial loading curve, (c) lower stresses during cyclic testing at 4% strain, and (d) lower stresses during stress relaxation testing at 4% strain. Data in Fig. 3b is from the same set as in Fig. 3a (focused in at the initial loading, or first few data points, to emphasize the rightward shift).

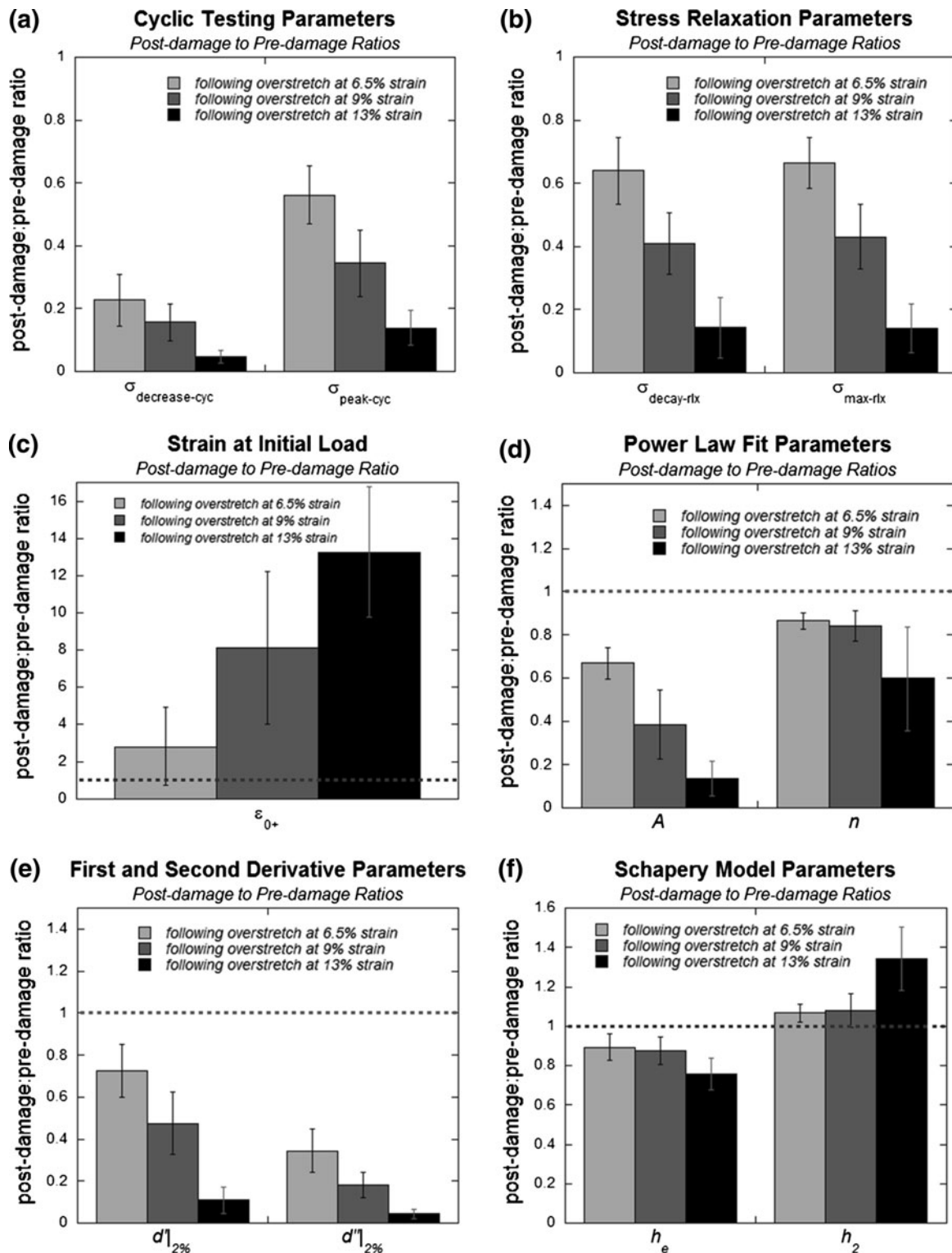


FIGURE 4. Post-damage to pre-damage ratio of mechanical parameters from cyclic (a, c, e) and relaxation (b, d, f) testing. (a) Cyclic testing parameters *stress decrease* (stress drop from first to tenth cycle) and *peak stress* (peak stress reached during cyclic testing to 4% strain); (b) relaxation testing parameters *stress decay* (stress decay over 100 s of relaxation testing) and *max stress* (maximum stress reached during step strain input of 4%); (c) stress–strain curve parameter *strain at initial load* (first strain value at which a nonzero load is reached); (d) power law fit parameters  $A$  and  $n$  (scalar multiplier and exponential from power law equation); (e) stress–strain curve parameters  $d^1l_{2\%}$  (first derivative of the stress–strain curve equation evaluated at 2% strain) and  $d^2l_{2\%}$  (second derivative of the stress–strain curve equation evaluated at 2% strain); (f) Schapery model parameters  $h_e$  and  $h_2$  (thermodynamic parameters used in the calculation of the Schapery model).<sup>12</sup> Error bars represent one standard deviation.

Stress–strain curve parameter  $\varepsilon_{0+}$ , representing the strain at which loading begins (and is therefore a measure of laxity), increases following overstretch (Fig. 4c). The post- to pre-damage ratios following overstretch to 6.5, 9, and 13% strain were  $2.82 \pm 2.08$ ,  $8.09 \pm 4.09$ , and  $13.26 \pm 3.51$ , respectively. Parameters from each overstretch strain were significantly different than the others ( $p = 0.0311$ ). The other stress–strain curve parameters,  $d'|_{2\%}$  and  $d''|_{2\%}$ , representing the slope of the stress–strain curve (first derivative) as well as its curvature (second derivative), both decreased following overstretch (Fig. 4e). Post- to pre-damage ratios of  $d'|_{2\%}$  were  $0.72 \pm 0.13$ ,  $0.48 \pm 0.15$ , and  $0.11 \pm 0.06$  following 6.5, 9, and 13% strain, respectively. Parameters at each of the overstretch strains was significantly different than the others ( $p = 0.0005$ ). Similarly, post- to pre-damage ratios of  $d''|_{2\%}$  were  $0.34 \pm 0.10$ ,  $0.18 \pm 0.06$ , and  $0.04 \pm 0.02$  following overstretch to 6.5, 9, and 13%, respectively. Again, parameters for each overstretch level were significantly different from each other ( $p = 0.0012$ ).

Power law fit parameters from the relaxation curve,  $A$  and  $n$ , both decrease following overstretch damage (Fig. 4d). Post- to pre-damage ratios following pull to 6.5, 9, and 13% strain for  $A$  were  $0.67 \pm 0.07$ ,  $0.38 \pm 0.16$ , and  $0.14 \pm 0.08$ ; parameters for each overstretch level were significantly different from each other ( $p = 0.0003$ ). Post- to pre-damage ratios for  $n$  were  $0.86 \pm 0.04$ ,  $0.84 \pm 0.07$ , and  $0.60 \pm 0.24$  for 6.5, 9, and 13% conditions. Parameters for each overstretch condition were significantly different from each other ( $p = 0.0078$ ).

Schapery model parameter  $h_e$  decreases following overstretch while the model parameter  $h_2$  increases

following overstretch (Fig. 4f). Ratios of post- to pre-damage parameter values for  $h_e$  were  $0.89 \pm 0.07$ ,  $0.87 \pm 0.07$ , and  $0.76 \pm 0.08$  following pulls to 6.5, 9, and 13% strain, and parameters for each overstretch level were significantly different from each other ( $p = 0.0082$ ). Post- to pre-damage parameter values for  $h_2$  had the opposite trend, with ratios of  $1.07 \pm 0.05$ ,  $1.09 \pm 0.09$ , and  $1.34 \pm 0.16$ . Parameters again were significantly different at each overstretch level ( $p = 0.0379$ ).

### Parameter Interrelationships: Objective 1

Interrelationships between parameters are displayed in Table 1. Strong correlations occurred between  $A$  and  $\sigma_{\max\text{-rlx}}$ ,  $\sigma_{\text{decay-rlx}}$ ,  $\sigma_{\text{peak-cyc}}$ , and  $d'|_{2\%}$ ; between  $\sigma_{\max\text{-rlx}}$  and  $\sigma_{\text{decay-rlx}}$ ,  $\sigma_{\text{peak-cyc}}$ , and  $d'|_{2\%}$ ; between  $\sigma_{\text{decay-rlx}}$  and  $\sigma_{\text{peak-cyc}}$ ; between  $\sigma_{\text{decrease-cyc}}$  and  $d'|_{2\%}$  and  $d''|_{2\%}$ ; and between  $d'|_{2\%}$  and  $d''|_{2\%}$ . Correlations existed between  $A$  and  $\sigma_{\text{decrease-cyc}}$ , and  $d''|_{2\%}$ ; between  $\sigma_{\max\text{-rlx}}$  and  $\sigma_{\text{decrease-cyc}}$ , and  $d''|_{2\%}$ ; between  $\sigma_{\text{decay-rlx}}$  and  $\sigma_{\text{decrease-cyc}}$ ,  $d'|_{2\%}$ , and  $d''|_{2\%}$ ; between  $\sigma_{\text{peak-cyc}}$  and  $\sigma_{\text{decrease-cyc}}$ ,  $d'|_{2\%}$ , and  $d''|_{2\%}$ ; and between  $h_e$  and  $h_2$ . Weak correlations existed between  $n$  and  $\sigma_{\max\text{-rlx}}$ ,  $\sigma_{\text{decay-rlx}}$ , and  $h_e$ ; between  $\sigma_{\max\text{-rlx}}$  and  $h_e$ ; and between  $d'|_{2\%}$  and  $h_e$ . Examples of parameter correlations for cyclic (Fig. 5a), stress relaxation (Fig. 5b), derivative (Fig. 5c), and Schapery model (Fig. 5d) ratios are shown in Fig. 5.

### Strain Dependence: Objective 2a

Power law fit parameters  $A$  and  $n$  increased with strain (Figs. 6a and 6b), Schapery model parameter  $h_e$  increased with strain (Fig. 6c) while model parameter  $h_2$

TABLE 1. Parameter relationships represented by  $R^2$  values of parameter–parameter plots.

	$A$	$n$	$\sigma_{\max\text{-rlx}}$	$\sigma_{\text{decay-rlx}}$	$\sigma_{\text{peak-cyc}}$	$\sigma_{\text{decrease-cyc}}$	$d' _{2\%}$	$d'' _{2\%}$	$\varepsilon_{0+}$	$h_e$	$h_2$
$A$	–	0.363	<b>0.927</b>	<b>0.877</b>	<b>0.878</b>	0.7636	<b>0.8502</b>	0.7979	[0.2479]	0.3196	[0.2205]
$n$		–	0.412	0.4306	0.242	0.3685	0.3893	0.2592	[0.0987]	0.4431	[0.3199]
$\sigma_{\max\text{-rlx}}$			–	<b>0.9419</b>	<b>0.892</b>	0.7304	<b>0.8212</b>	0.7733	[0.2783]	0.4123	[0.3499]
$\sigma_{\text{decay-rlx}}$				–	<b>0.883</b>	0.6322	0.7023	0.6314	[0.2998]	0.3548	[0.2939]
$\sigma_{\text{peak-cyc}}$					–	0.6745	0.7397	0.7341	[0.3295]	0.2592	[0.2051]
$\sigma_{\text{decrease-cyc}}$						–	<b>0.8967</b>	<b>0.8664</b>	[0.2272]	0.3672	[0.1796]
$d' _{2\%}$							–	<b>0.9223</b>	[0.2076]	0.4469	[0.2504]
$d'' _{2\%}$								–	[0.1901]	0.3554	[0.1998]
$\varepsilon_{0+}$									–	[0.1586]	0.123
$h_e$										–	[0.6881]
$h_2$											–

Parameters:  $A$  (overall stiffness) and  $n$  (relaxation rate) from power law fit;  $\sigma_{\max\text{-rlx}}$  (maximum stress reached) and  $\sigma_{\text{decay-rlx}}$  (decrease in stress over 100 s) from relaxation curves;  $\sigma_{\text{peak-cyc}}$  (peak stress reached) and  $\sigma_{\text{decrease-cyc}}$  (decrease in peak stress over 10 cycles) from cyclic test results;  $d'|_{2\%}$  (slope/first derivative of curve),  $d''|_{2\%}$  (curvature/second derivative of curve), and  $\varepsilon_{0+}$  (strain at load onset) from stress–strain curves;  $h_e$  and  $h_2$  from Schapery's nonlinear viscoelastic model calculations.

[–] = negative correlation (opposing trends).

Bold represents strongly correlated parameters  $R^2 > 0.8$ .

decreased with strain (Fig. 6d), maximum stress reached during relaxation increased with strain (Fig. 6e), and the stress decay over 100 s of relaxation decreased with strain (Fig. 6f). In each case, the trend for *decreasing* strain matched the trend for *increasing* “damage strain” (strain input during overstretch).

#### Equivalent Strain Calculations: Objective 2b

The effective strain equivalent for each parameter, plotted in Fig. 7, was reduced from the applied strain (4%) in each case, and was reduced the most following the greatest overstretch strain input (13%), least following the least overstretch strain input (6.5%).

When averaged across all of the modeling parameters, the average effective strains were  $2.43 \pm 0.33$ ,  $1.98 \pm 0.3$ , and  $0.88 \pm 0.43\%$  following overstretch strain inputs of 6.5, 9, and 13%. All model parameter values ( $A$ ,  $n$ ,  $h_e$ , and  $h_2$ ) were within a standard deviation of the mean effective strain value (Fig. 8).

#### Model Calculations: Objective 2c

The ratio of effective strain to applied strain as a function of overstretch strain was plotted (Fig. 9a) to empirically determine the constant,  $C$ , for the damage

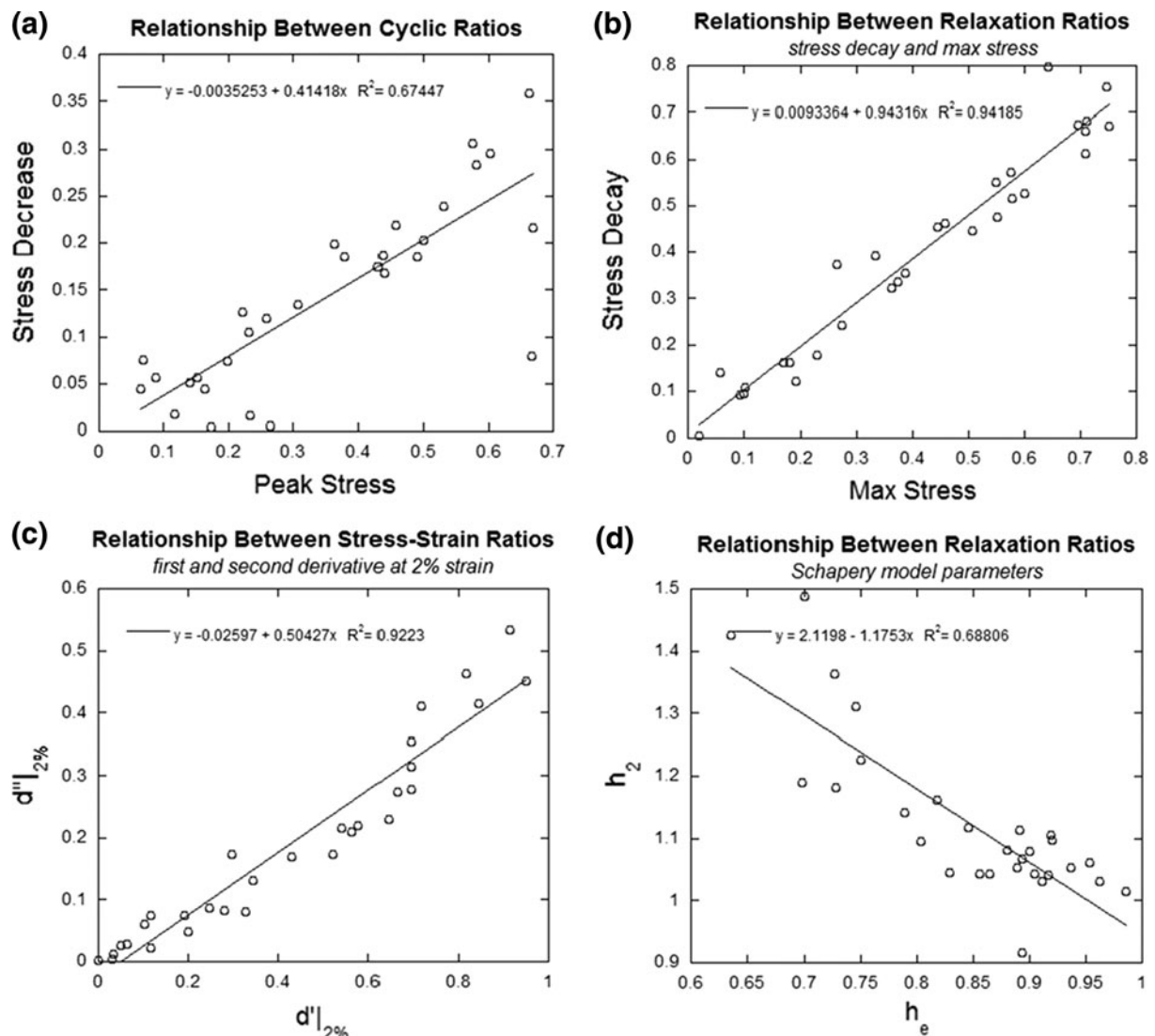


FIGURE 5. Parameter relationship plots for (a) cyclic ratios ( $\sigma_{\text{peak-cyc}}$  and  $\sigma_{\text{decrease-cyc}}$ ), (b) stress relaxation ratios ( $\sigma_{\text{max-rlx}}$  and  $\sigma_{\text{decay-rlx}}$ ), (c) derivative ratios ( $d'l_{2\%}$  and  $d''l_{2\%}$ ), and (d) Schapery model ratios ( $h_e$  and  $h_2$ ). For a complete list of correlations, see Table 1.

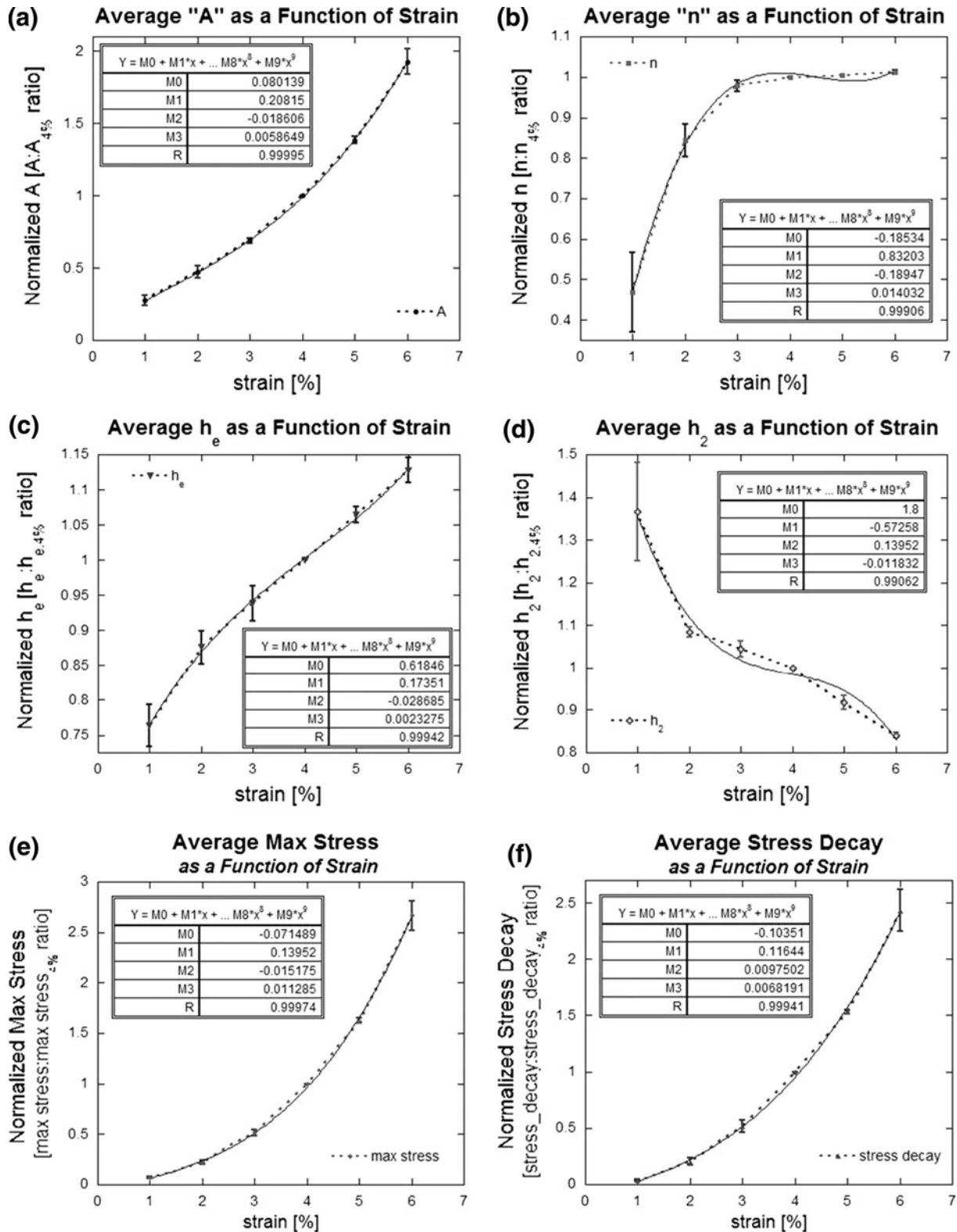


FIGURE 6. Normalized (by 4% strain test values) parameters as a function of strain and fitted with third-order polynomial (of the form  $M0x^3 + M1x^2 + M2x + M3$ ), including power law parameter fits (a, b), Schapery model parameter fits (c, d), average maximum stress reached (e), and stress decay over 100 s (f). Error bars indicate standard error ( $n = 5$ ).

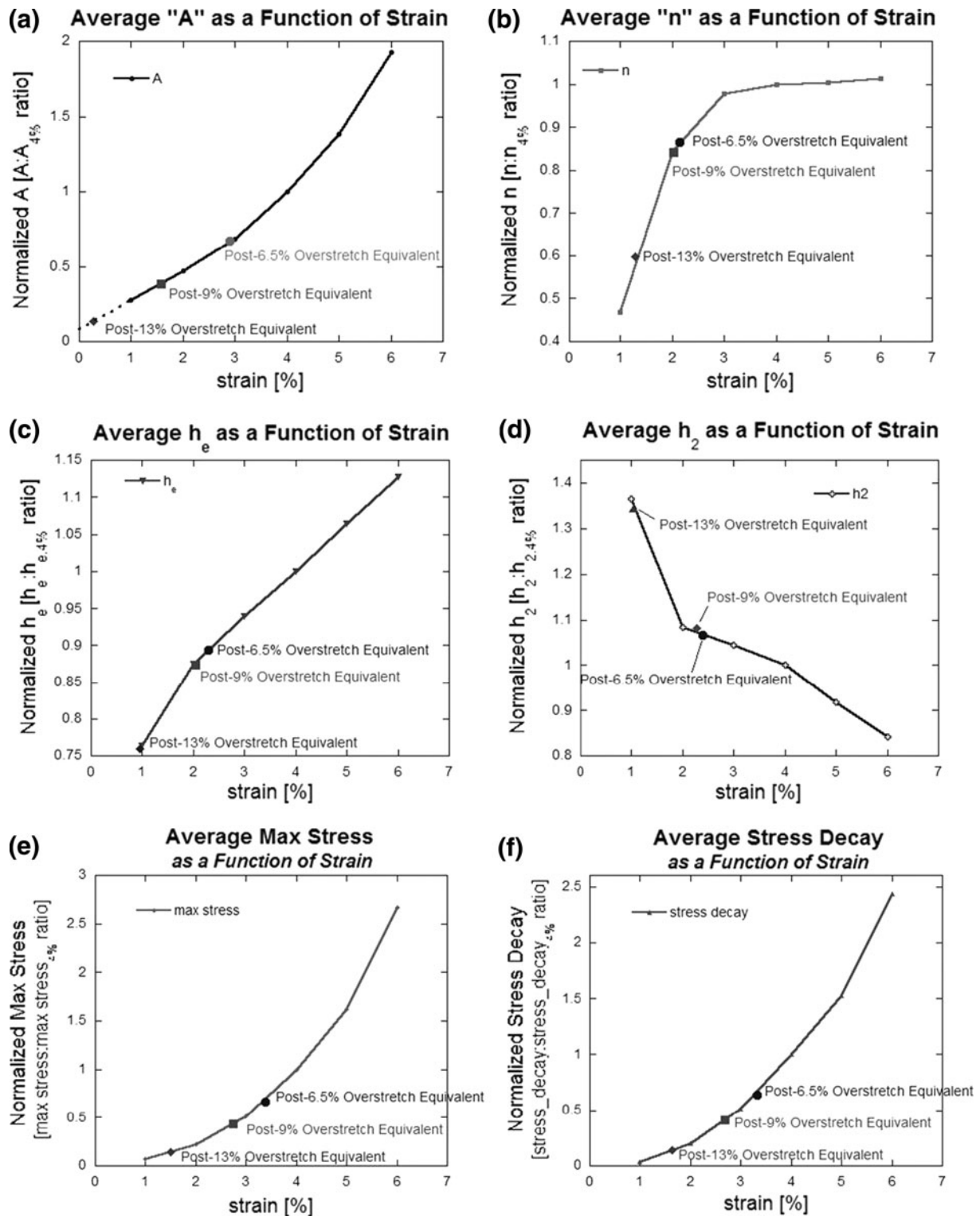


FIGURE 7. Effective strain equivalent for parameters following overstretch strain of 6.5, 9, and 13% for power law parameter fits (a, b), Schapery model parameter fits (c, d), average maximum stress reached (e), and stress decay over 100 s (f).

parameter in Eq. (12). The same ratio was plotted as a function of the post-damage to pre-damage slope ratios (Fig. 9b) to verify that these values are correlated in the manner outlined in Eq. (13).

The empirical value,  $C$ , was found to be 0.059, resulting in the final equation:

$$\epsilon_{\text{eff}} = 0.04[1 - 0.059 (\text{strain input})] \quad (16)$$

This equation was used to calculate the “empirical” model, while Eq. (13) was used to calculate the “slope” model. Calculated parameter values are plotted with actual data values in Fig. 10.

The models calculated using these parameters, as well as a Schapery model fit from the post-damage data, is plotted in Fig. 11. All models characterized the

stress relaxation behavior reasonably well following overstretch to 6.5 (Fig. 11a), 9 (Fig. 11b), and 13% (Fig. 11c); the Schapery model fit constructed from actual data values had the least error (Fig. 11d; Table 2), as would be anticipated, but the average percent error was not significantly different between models for any overstretch damage case (post-6.5%,  $p = 0.181$ ; post-9%,  $p = 0.521$ ; post-13%,  $p = 0.227$ ; overall,  $p = 0.856$ ).

DISCUSSION

Despite their uniaxial loading and simple appearance, tendons are natural composite materials with intricate microstructures and complex mechanical behaviors. Understanding how these behaviors change following damage is critical for understanding mechanical function, quantifying compromise with subfailure damage, and benchmarking normal functional behaviors to evaluate the efficacy of injury treatments. Understanding changes in laxity experienced by post-damage tendons better helps elucidate how muscles must compensate, as well as anticipate the potential for abnormal neuromuscular control of movements.

In this study, we found that elastic parameters  $\sigma_{peak-cyc}$  and  $\sigma_{max-rlx}$  were decreased following overstretch (Fig. 2). This indicates that the tendon has less resistance to deformation after sustaining subfailure damage. Tendons and ligaments have a strain-stiffening stress-strain curve, which leads to greater resistance to deformation as strain in the tendon increases; this behavior allows tendons and ligaments to control joint

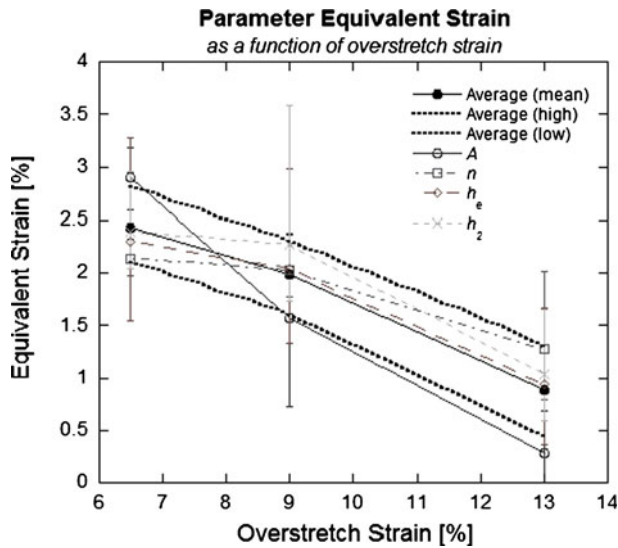


FIGURE 8. Equivalent strain values for modeling parameters  $A$  (overall stiffness),  $n$  (relaxation slope),  $h_e$ , and  $h_2$ . “Average (mean)” indicates the mean equivalent strain value across all parameters, “Average (high)” indicates the mean equivalent strain value + 1 standard deviation, and “Average (low)” indicates the mean equivalent - 1 standard deviation. Error bars indicate one standard deviation (of parameter equivalent strain mean). Parameter equivalent strain values fall within one standard deviation of the mean equivalent strain value.

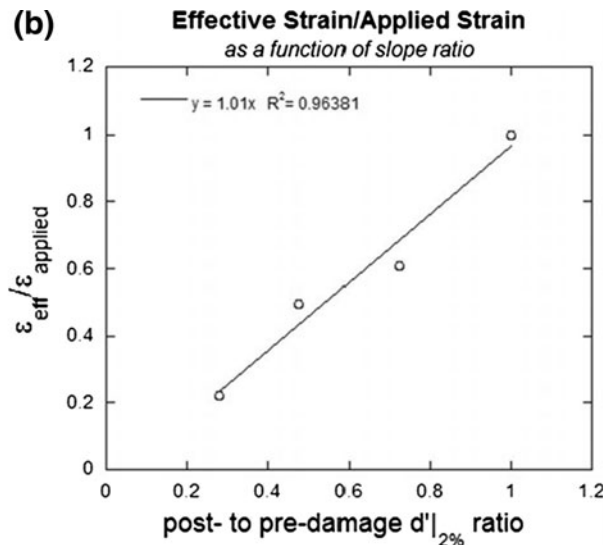
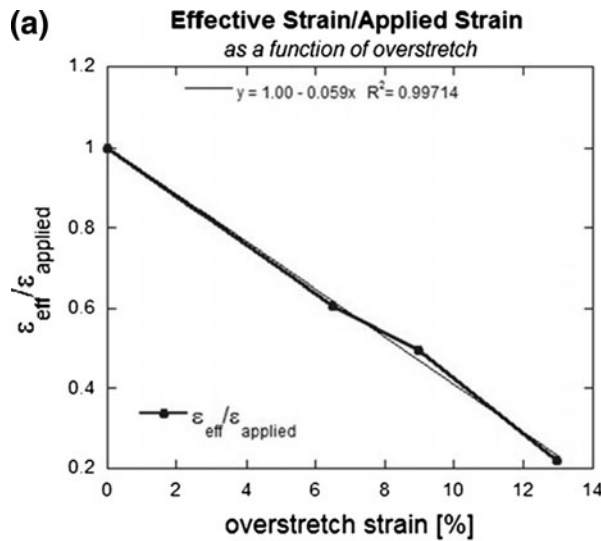


FIGURE 9. Effective strain/applied strain ratio as a function of (a) overstretch strain and (b) post-damage to pre-damage slope ratio. The resulting value of  $C$  is 0.059. The relationship between effective strain and slope is confirmed.

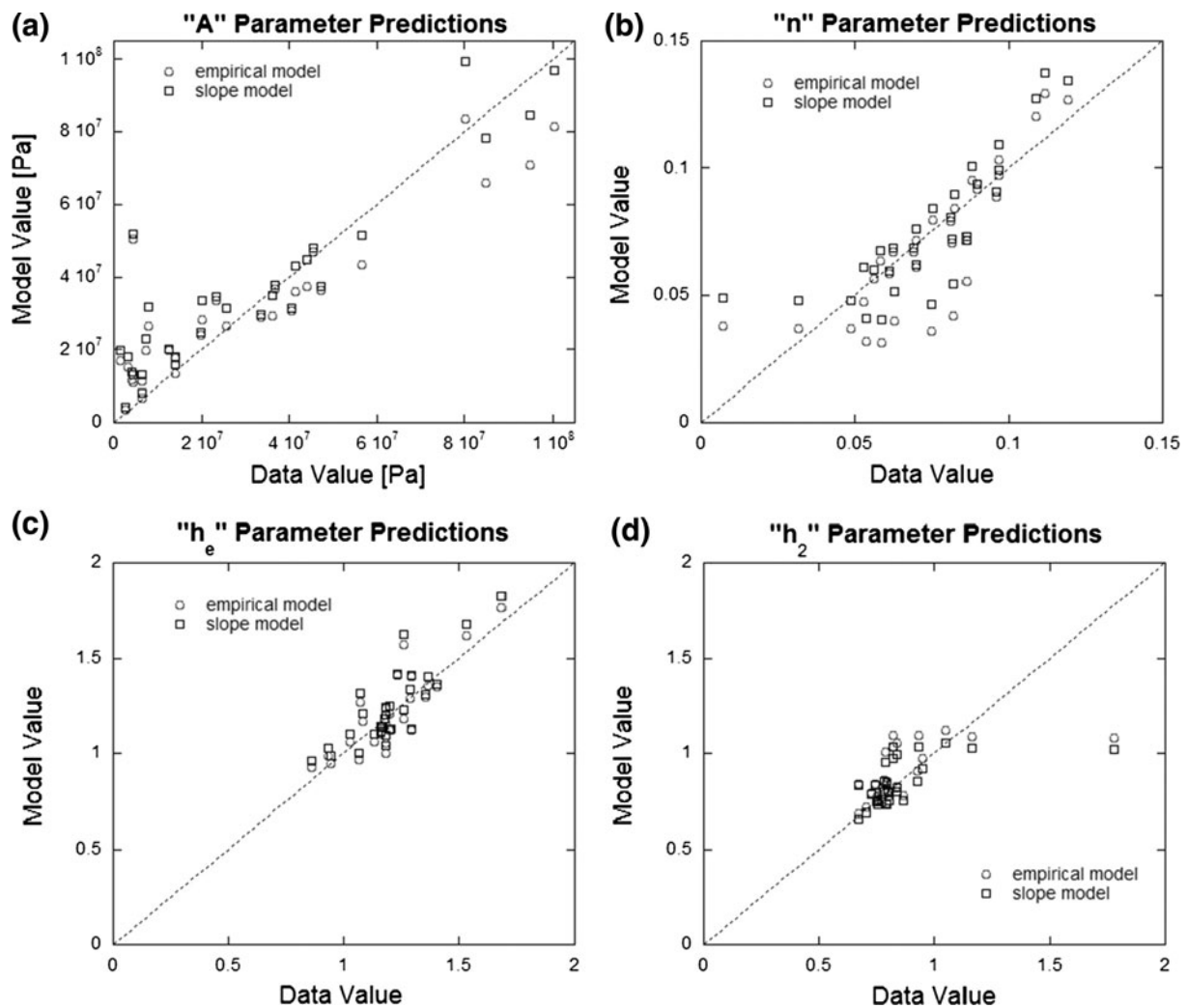


FIGURE 10. Parameter predictions based on empirical and slope models for (a)  $A$ , (b)  $n$ , (c)  $h_e$ , and (d)  $h_2$  values. The dotted diagonal line has a slope of 1 and represents the point at which the model and data values are equivalent.

kinematics by resisting excessive movement of the joint as well as facilitating more efficient transfer from muscle flexion to bone movement. Increased tendon laxity resulting from subfailure damage therefore reduces the tendon's ability to resist excessive movement, which increases the potential for further damage and ultimate tendon failure with time or chronic degenerative joint disease.

Similarly, the viscoelastic parameters  $\sigma_{\text{decay-rlx}}$  and  $\sigma_{\text{decrease-cyc}}$  (Fig. 2) decreased following overstretch damage. This means that the time-dependent properties have been altered. Specifically, damage reduces the relaxation and the dynamic softening under cyclic load. This will affect the ability of the tendons to respond to loading situations over time. We also see that energy absorption is reduced by damage. Functional implications of this are substantial. From a microstructural and molecular perspective, alterations

in viscoelastic properties indicate changes in the interactions between the components within the tendon.

Parameters describing the shape of the stress-strain curve,  $d'|_{2\%}$  (slope of stress-strain curve) and  $d''|_{2\%}$  (curvature of stress-strain curve) also decreased following overstretch damage. This is a quantifiable measure of the changes that occur in the stress-strain curve following damage, and is indicative of laxity in the tissue. Another measure of the changes to the stress-strain curve is  $\varepsilon_{0+}$ , the strain at which the tendon picks up load. An increase in this variable indicates a quantifiable rightward shift of the stress-strain curve, and another manifestation of laxity.

Relaxation curve power law fit parameters  $A$  and  $n$  consistently decreased following overstretch, which means the tendon became overall more compliant (lower  $A$ ) and less viscoelastic (lower  $n$ ). This is not surprising, as stress reached and stress decay during

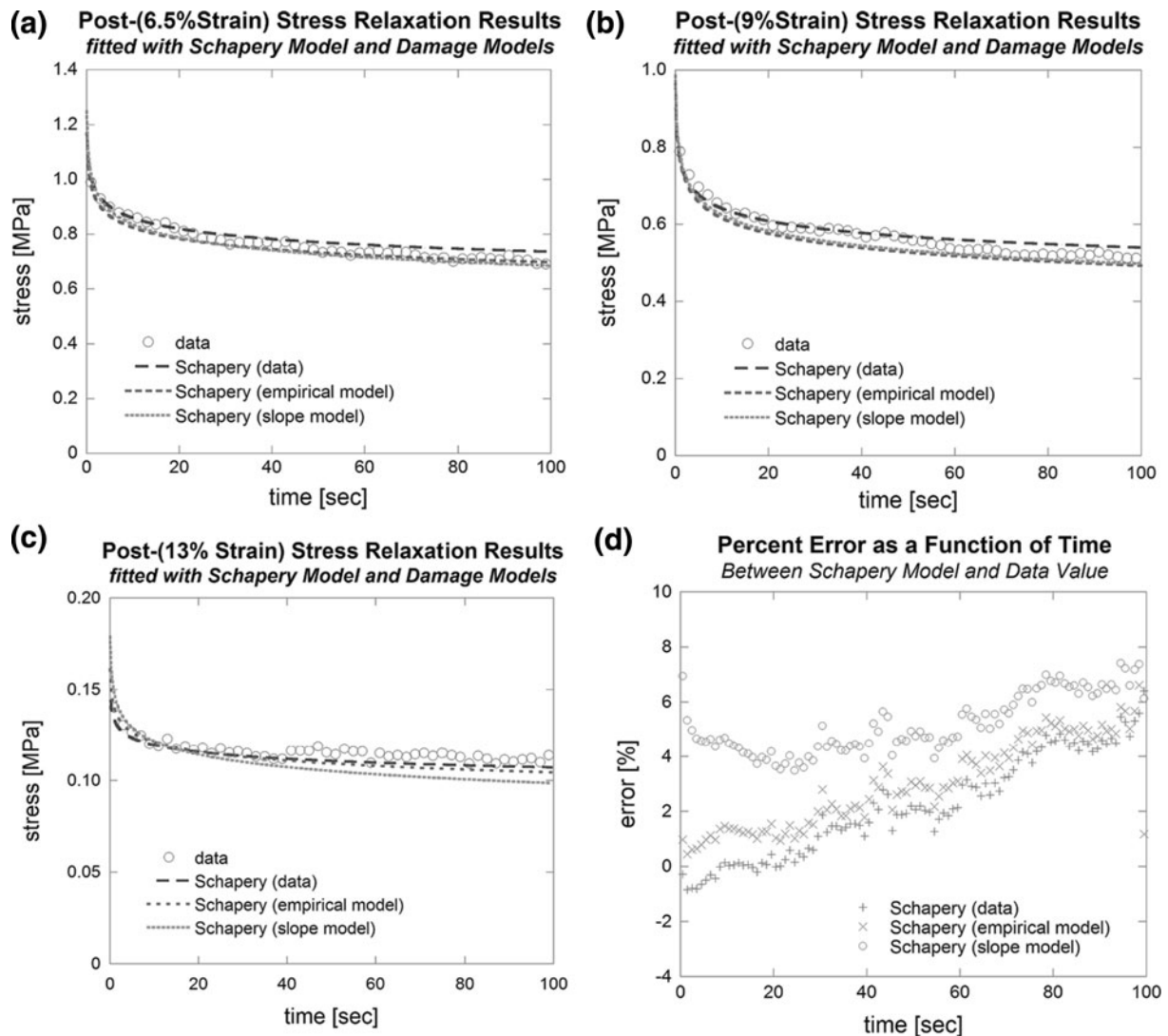


FIGURE 11. Schapery model calculated with parameters from data fit, empirical model, and slope model. All models fit the data for (a) post-6.5% strain data, (b) post-9% strain data, and (c) post-13% data reasonably well, with (d) overall percent error less than 10% for each model. For visibility, every 10th data point is shown.

TABLE 2. Percent error between Schapery model value and actual data value.

	Percent error			
	Post-6.5%	Post-9%	Post-13%	Overall
Data	2.69	1.80	2.05	2.18
Empirical	-12.75	-3.11	24.94	3.02
Slope	-4.41	-1.97	21.96	5.19

stress relaxation are decreased, and resulting curve fits of the relaxation modulus would likely decrease accordingly. While  $A$  ratio values (representing overall stiffness) consistently correlated to other stress relaxation parameters, as expected,  $n$  ratio values (representing relaxation rate correlated weakly or not at all to other parameters. This is likely due in part to the

linear nature of the correlation (a nonlinear relationship would result in a poor linear correlation fit).

Schapery model parameter  $h_2$  consistently increases following overstretch, and parameter  $h_e$  consistently decreases following overstretch. This implies that constitutive models, given an understanding of how parameters change following damage and an estimate of damage level, can be altered to relate damage to post-damage stress and/or strain levels.

The amounts that each of these parameters decreased depended on the strain during overstretch, indicating that the amount of diffuse damage in a tendon can be varied by varying the strain used to create it. It also means that mechanical properties of tendon can be indicative of the level of damage in the tendon and implies that it may be possible to correlate mechanical parameters, both viscoelastic and elastic,

to the damage state of the tissue. In this manner, it would be possible to diagnose diffuse damage in the tissue while it is still intact and predict risk of additional injury with continued function. With increasing popularity and capabilities of noninvasive force measurements, there is potential for measurement of diffuse damage *in vivo*, which is currently not possible using imaging modalities such as conventional MRI or ultrasound (unlike focal defect damages which are readily visualized by such technologies).

The stress relaxation behavior of tendons was modeled by determining the equivalent strain experienced by the tendons following subfailure damage induced by overstretch to 6.5, 9, or 13% strain. Using the calculated strain-dependent behaviors of the various parameters, the equivalent strain could be substituted in for applied strain and thus the post-damage parameters could be calculated and used for model calculations. While this study only demonstrated the ability to fit stress relaxation behavior with Schapery's viscoelastic model, this "equivalent strain" approach could be used in any constitutive model provided the parameter strain-dependence is known.

While this equivalent strain approach does a good job of modeling the mechanical compromise that exists immediately after overstretch, it has a few inherent limitations. First, it only considers the post-damage mechanical properties gathered in the time window immediately after damage (~17 min–1 h). We have previously shown that the recovery from moderate loading occurs slowly, requiring more time to fully recover from loading than the length of the loading test.<sup>1</sup> It is not unreasonable to assume that the recovery following large strains would require an even longer time period (on the order of several hours or more) to fully recover the mechanical parameters. Thus, damage could potentially be described as a function of time, with partial recovery of mechanical properties possible over extended periods of time, independent of biological repair that would occur *in vivo*.

A second limitation is the lack of consideration of the biological response to overstretch, which is an important factor in *in vivo* injury response. During the short time period examined in this study, there would likely be limited effects due to cellular response, but ultimately the healing and remodeling response of the tendon would likely alter both the elastic and viscoelastic properties over time.

An interesting result is the fact that the magnitude of the error between test data and the models is larger following a pull to 13% strain than either 6.5 or 9% strain. This is likely due to the fact that as the failure strain (reported to be 15–20%<sup>5,12</sup>) is approached, the model moves from a subfailure, microdamage model

(seen after pulls to 6.5 or 9% strain) to a partial failure, macrodamage model. Due to biologic variation, some tendons may be nearly failed at 13% while others are still only sustaining microdamage.

Diffuse damage induced by deforming tendons to strains outside of normal activity (but less than failure strain) affects a multitude of parameters. Elastic and viscoelastic parameters, obtained during stress relaxation and cyclic testing, were significantly decreased following damage. Furthermore, these effects become more pronounced as the strain during the overstretch pull increases. The strain-dependent mechanical parameters of tendons after subfailure damage behaved as if the tendon was being pulled to a lower strain level, validating the use of an effective strain model. By determining the effective strain level and using it to calculate predicted values of post-damage mechanical parameters, it was possible using both the overstretch strain value as well as the ratio of the post-damage to pre-damage stress–strain curve slopes to predict the stress relaxation behavior of the tendon with the Schapery nonlinear viscoelastic model. Thus, if the strain-dependence of the parameters can be determined, it is possible to anticipate the post-damage mechanical behavior of tendons. The slope-based estimation of effective strain holds particular promise, as a stress–strain curve can be generated following damage induced by methods other than overstretch, and thus estimation of effective strain in this manner can be pursued for damage caused by methods such as repetitive loading or laceration. Additionally, as methods for noninvasive loading and strain measurement improve, information from a stress–strain curve can be used to estimate a multitude of mechanical parameters to better assess tissue function following injury.

In conclusion, we have quantified how elastic and viscoelastic behaviors in tendon are altered as a function of subfailure overstretch, how these behavior changes can be interpreted as damage, and how these damage-induced changes in parameters are interrelated. This altered response can be described by the effective strain model, in which the tendon is modeled as if it were being pulled to a lower (effective) strain. We have demonstrated that a single, measurable parameter (effective strain) can account for all of the elastic and viscoelastic changes with damage, and robustly be predictive of tendon behavior. Finally, we have modeled these behavior changes with a nonlinear viscoelastic model (Schapery's nonlinear viscoelastic model). Such experiments and modeling develop a better understanding of tendon mechanics and better anticipate the sequelae of such events *in vivo*.

### ACKNOWLEDGMENTS

This work was funded by NSF award 0553016. The authors would like to thank Ron McCabe for his technical assistance.

### REFERENCES

- <sup>1</sup>Duenwald, S. E., R. Vanderby, and R. S. Lakes. Viscoelastic relaxation and recovery of tendon. *Ann. Biomed. Eng.* 37(6):1131–1140, 2009.
- <sup>2</sup>Duenwald, S. E., R. Vanderby, and R. S. Lakes. Stress relaxation and recovery in tendon and ligament: experiment and modeling. *Biorheology* 47(1):1–14, 2010.
- <sup>3</sup>Gardiner, J. C., J. A. Weiss, and T. D. Rosenberg. Strain in the human medial collateral ligament during valgus loading of the knee. *Clin. Orthop. Relat. Res.* 391:266–274, 2001.
- <sup>4</sup>Hokanson, J., and S. Yazdani. A constitutive model of the artery with damage. *Mech. Res. Commun.* 24(2):151–159, 1997.
- <sup>5</sup>Johnson, G. A., D. M. Tramaglino, R. E. Levine, K. Ohno, N. Y. Choi, and S. L. Woo. Tensile and viscoelastic properties of human patellar tendon. *J. Orthop. Res.* 12(6):796–803, 1994.
- <sup>6</sup>Lemaitre, J. How to use damage mechanics. *Nucl. Eng. Des.* 80(2):233–245, 1984.
- <sup>7</sup>Lochner, F. K., D. W. Milne, E. J. Mills, and J. J. Groom. In vivo and in vitro measurement of tendon strain in the horse. *Am. J. Vet. Res.* 41(12):1929–1937, 1980.
- <sup>8</sup>Natali, A. N., P. G. Pavan, E. L. Carniel, M. E. Lucisano, and G. Tagliavero. Anisotropic elasto-damage constitutive model for the biomechanical analysis of tendons. *Med. Eng. Phys.* 27(3):209–214, 2005.
- <sup>9</sup>Perry, S. M., C. L. Getz, and L. J. Soslowsky. After rotator cuff tears, the remaining (intact) tendons are mechanically altered. *J. Shoulder Elbow Surg.* 18(1):52–57, 2009.
- <sup>10</sup>Provenzano, P. P., D. Heisey, K. Hayashi, R. Lakes, and R. Vanderby. Subfailure damage in ligament: a structural and cellular evaluation. *J. Appl. Physiol.* 92(1):362–371, 2002.
- <sup>11</sup>Schapery, R. A. On the characterization of nonlinear viscoelastic materials. *Polym. Eng. Sci.* 9(4):295–310, 1969.
- <sup>12</sup>Shadwick, R. E. Elastic energy storage in tendons: mechanical differences related to function and age. *J. Appl. Physiol.* 68(3):1033–1040, 1990.
- <sup>13</sup>Simo, J. C. On a fully three-dimensional finite-strain viscoelastic damage model: formulation and computational aspects. *Comput. Methods Appl. Mech. Eng.* 60(2):153–173, 1987.